

Observation of angle-dependent transmission of Dirac electrons in graphene heterojunctions

Atikur Rahman, Janice Wynn Guikema, N. M. Hassan, and Nina Marković

Department of Physics and Astronomy, Johns Hopkins University, Baltimore, Maryland 21218, USA.

The relativistic nature of charge carriers in graphene is expected to lead to an angle-dependent transmission through a potential barrier, where Klein tunneling involves annihilation of an electron and a hole at the edges of the barrier. The signatures of Klein tunneling have been observed in gated graphene devices, but the angle dependence of the transmission probability has not been directly observed. Here we show measurements of the angle-dependent transmission through quasi-ballistic graphene heterojunctions with straight and angled leads, in which the barrier height is controlled by a shared gate electrode. Using a balanced differential measurement technique, we isolate the angle-dependent contribution to the resistance from other angle-insensitive, gate-dependent and device-dependent effects. We find large oscillations in the transmission as a function of the barrier height in the case of Klein tunneling at a 45° angle, as compared to normal incidence. Our results are consistent with the model that predicts oscillations of the transmission probability due to interference of chiral carriers in a ballistic barrier. The observed angle dependence is the key element behind focusing of electrons and the realization of a Veselago lens in graphene.

Charge carriers in graphene behave like massless, relativistic particles [1–4], characterized by chirality which arises from the existence of two interpenetrating sublattices in the hexagonal crystal structure of graphene. Due to the chiral nature of the charge carriers, back scattering by impurities is forbidden [5, 6], giving rise to unusual effects in graphene p-n-p junctions such as Klein tunneling, electron lensing and collimation [7–24]. As a consequence of the charge conjugation-like symmetry between electrons and holes, Klein tunneling in graphene involves annihilation of an electron and a hole at each p-n interface [10]. For a ballistic p-n-p junction with sharp edges ($k_F t < 1$, where t is the distance over which the potential increases at the p-n interface, and k_F is the Fermi wavevector), the transmission probability is equal to unity for normally incident charge carriers (incident angle $\phi = 0^\circ$, with respect to the junction normal). Away from the normal incidence ($\phi \neq 0$), the transmission probability is expected to oscillate as a function of the incident angle for a fixed barrier height [10]. For

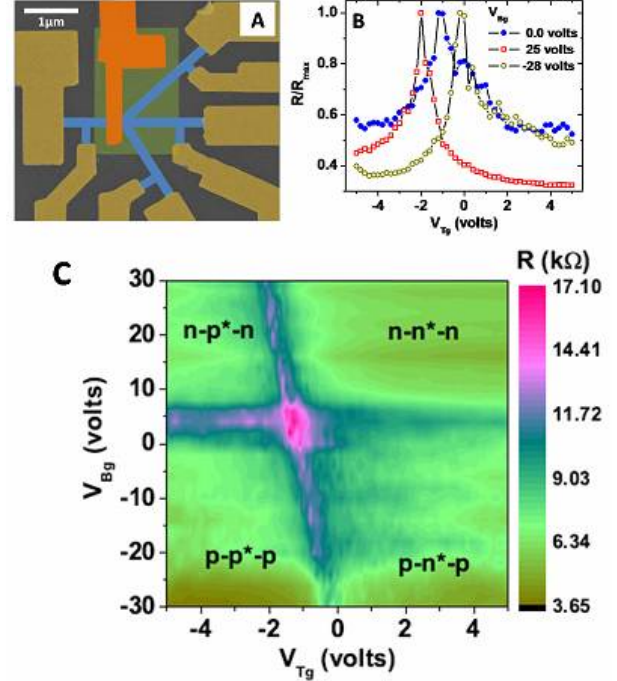


FIG. 1: (A) False color SEM micrograph of a patterned single layer graphene device with straight and angled arms (blue). The straight arms are perpendicular to the top gate, and the angled arms form a 45° angle with the top gate. The top gate (shown in orange) is placed at the point where the straight and angled arms meet. The gate dielectric is shown in green (20 nm of Al_2O_3), and the leads are yellow (5nm Cr/ 75nm Au). The resistance of each arm is measured in a four-probe configuration using non-invasive leads [31]. The scale bar is 1 μm long. (B) Normalized resistance as a function of the top gate voltage for three different values of back gate voltage measured on the straight arm (device SL1). (C) Color plot of the resistance as a function of back gate and top gate voltage measured on the straight arm (device SL2). The dark lines trace the shift of the charge neutrality point as a function of V_{Bg} and V_{Tg} , defining regimes in which the device forms an n-p-n, n-n-n, p-p-p or a p-n-p structure, as labeled.

a fixed incident angle, other than normal incidence, the transmission probability also oscillates with varying barrier height. However, realistic experimental configurations typically involve smooth junctions ($k_F t > 1$) which focus electrons quite effectively, and the transmission is expected to be strongly suppressed as the incident angle increases [8]. Effects of disorder [25] and screening [26] are also always present in realistic systems and need to be taken into account.

Signatures of Klein tunneling in graphene have been reported before in gated graphene devices. Asymmetry in the resistance with respect to the gate voltage has been attributed to the difference between the Klein tunneling and over-barrier transmission [18, 19, 27]. Measurements on ballistic p-n-p junctions were shown to have larger resistance than the diffusive ones [22], and electron guiding has been demonstrated based on angle-selective transmission through a p-n interface [23]. In the coherent ballistic regime, conductance oscillations as a function of gate voltage have been interpreted as tunneling through quasi-bound states formed by Fabry-Perot interference between wavefunctions scattered forward and backward between the two p-n interfaces [11, 20, 21]. In contrast, direct and unambiguous evidence of the angle dependence of transmission through a p-n-p junction is still lacking. Sutar et al. [24] studied the resistance of p-n-p junctions with angled gates, finding that the junction resistance increases as the angle of the gate is increased from normal incidence. However, the experiments are typically done in the two-terminal geometry [18–24], in which case the contact effects are unavoidable [21, 28–31] and can be difficult to take into account. Even the four-probe measurements in graphene can be problematic due to doping from the leads [18]. In addition, to study the angle dependence directly, one typically has to compare different physical samples. In such cases, direct comparison is often obscured by inevitable differences in the structure and the level of disorder.

Here we report a measurement of angle-dependent transmission as a function of barrier height across graphene p-n-p (or n-p-n) junctions. The device geometry (shown in Fig. 1A) and a balanced differential measurement technique were specifically designed to separate out the angle-dependent effects from other gate-dependent, but angle-insensitive resistances.

Graphene flakes were mechanically exfoliated from natural flake graphite and deposited on a Si wafer coated with 300 nm SiO₂ [1, 2]. Single-layer flakes were identified by optical microscope and confirmed by Raman spectroscopy. Electrical leads were patterned by standard optical and e-beam lithography and the contacts were thermally evaporated (5nm Cr/ 75nm Au). Oxygen plasma (100 W for 45 sec) was used to pattern the graphene. To fabricate the top gate, 20 nm of Al₂O₃ was deposited as the top gate insulating layer, followed by deposition of a 200 nm wide gold electrode on top. Scanning electron microscope (SEM) image of a typical device is shown in Fig. 1A. The mobility in our samples is ~ 2800 cm²/Vs, which is typical for graphene on SiO₂ substrates. This implies an average impurity concentration of 10^{10} cm⁻² [25].

Electrical measurements were carried out at 4.2 K by placing the samples in vacuum in a He3 cryostat. The bias current was kept sufficiently low to avoid heating. Measurements were done in a four probe geometry

with external voltage probes [31], using the SR 560 low noise preamplifier and PAR 124A analog lock-in amplifier equipped with an EG&G 116 preamplifier (operating in differential mode).

The resistance as a function of the back gate voltage (V_{Bg}) and the top gate voltage (V_{Tg}) is shown in Fig. 1B and 1C for a typical device, measured on the straight arm at 4.2 K. Normalized resistance as a function of V_{Tg} is shown in Fig. 1B for three values of V_{Bg} . For $V_{Bg} = 0$, the resistance is symmetric around the Dirac point, while for large positive and negative V_{Bg} , it shows an asymmetry that has also been observed by others [18]. Specifically, a larger resistance is found for the values of V_{Tg} that induce carriers of the opposite polarity under the top gate, forming a p-n-p or an n-p-n junction. With a suitable combination of V_{Bg} and V_{Tg} , all portions of the graphene device can be p or n type, or one can make a p-n-p or an n-p-n structure, as indicated in Fig. 1C. The two crossing dark lines in Fig. 1C trace the resistance peaks corresponding to the Dirac points as a function of the top and back gate voltage, showing the regions of neutrality in the sample. The slope of the diagonal line, dV_{Bg}/dV_{Tg} (~ 30 in our samples), represents the efficiency of the top gate control of the carrier density as compared to that of the back gate.

Our graphene device has four arms, one on the left side of the top gate (1) and three on the right side (2, 3 and 4). The top gate is placed over arm 1, just before the point at which arms 2, 3 and 4 branch out at different angles (arm 2 at 0°, and arms 3 and 4 at $\pm 45^\circ$). The resistance as a function of V_{Tg} for $V_{Bg} = 30$ volts, measured between arm 1 and each of the other three arms (in a standard four-probe configuration using non-invasive leads [31]) is shown in Fig. 2A. Since the three current paths share a common top-gated portion, the effect of the top gate on all three arms is almost identical. Any angle-dependent portion of this resistance would be included in the difference in the resistance as a function of V_{Tg} of the straight arm and either of the angled arms, $R_2(V_{Tg}) - R_3(V_{Tg})$, or $R_2(V_{Tg}) - R_4(V_{Tg})$, but *not* in $R_3(V_{Tg}) - R_4(V_{Tg})$ (arms 3 and 4 are both at $\pm 45^\circ$), so the angle-dependent contribution should be identical). However, this difference would also include other angle-independent contributions (minor differences in size, geometry, or impurity configuration). As is evident in Fig. 2A, this difference is quite small, and also shows mesoscopic fluctuations that are typically observed in samples of this size [32].

In order to separate out the angle-dependent contribution, we use a balanced differential measurement as shown in the schematic in Fig. 2B. In each measurement, the current bias is applied between arm 1 and two of the arms on the right of the top gate, either one straight and one angled arm, or two angled arms (the schematic in Fig. 2B shows measurements that compare arms 2 and 3, while arm 4 is not connected). The resistances of the two paths are then balanced with the help of a variable

resistor so that the voltage difference ΔV between the two paths for $V_{Tg} = 0$ is zero (limited by the background noise of a few nanovolts). The relevant resistances and the current branching schematic are shown in Fig. 2C. The resistance R_1 of arm 1 and the resistance of the entire p-n-p junction R_J under the top gate are included in both current paths, and the resistances $R_2 = R_{2b} + R_{2d}$ and $R_3 = R_{3b} + R_{3d}$ will determine the current branching between the arms 2 and 3 at $V_{Tg} = 0$ (here R_{2b} and R_{3b} are the resistances of the ballistic portions of the leads that are within the mean free path of the right p-n interface, while R_{2d} and R_{3d} are the resistances of the remaining diffusive portions of the leads). A differential measurement of the voltage drop between the two paths cancels out any common mode signal, including R_1 , R_J and any external noise that affects both paths equally. Balancing the two arms at $V_{Tg} = 0$ ensures that $\Delta V = I_2(V_{Tg} = 0)R_2 - I_3(V_{Tg} = 0)R_3 = 0$, with R_1 and R_J cancelling out (being common to both paths). Applying a voltage to the top gate changes only the resistance under the top gate R_J , which is shared by both paths and will not cause a deviation from the balanced condition - therefore, we are *not* measuring the resistance of the p-n-p junction, or either of the two p-n interfaces (all of which are common to both paths). A deviation from the balanced condition, $\Delta \neq 0$, can only be caused by a redistribution of current between arms 2 and 3 as a function of the top gate. The current branching in arms 2 and 3 is determined by R_2 and R_3 , neither of which is directly affected by V_{Tg} - any differences in geometry, size, impurity configurations and resistivity in the two arms are already cancelled out by balancing R_2 and R_3 , and neither arm is under the top gate. If, however, there were any gate-dependent difference in the transmission probability between the two arms, it would affect the distribution of current in the arms 2 and 3 within the distance from the junction of the order of the mean free path. More specifically, it would affect the current distribution through R_{2b} and R_{3b} , causing a difference in the voltage drop over R_{2b} and R_{3b} . This would cause a deviation $\Delta V(V_{Tg})$ from the balanced condition, which measures the difference in the voltage drop *only* over the ballistic portion ($\Delta V = I_2(V_{Tg})R_{2b} - I_3(V_{Tg})R_{3b}$). It is this deviation from the balanced condition that we measure below. In order to relate the measurement to the transmission probability, we define a parameter $R_{dev} = \Delta V(V_{Tg} = 0)/I_1$ with units of resistance. R_{dev} is then proportional to the difference in the transmission probability and reflects the current redistribution in the two leads as a function of V_{Tg} .

For a particular back gate voltage, we begin by balancing two of the arms (2 and 3) at $V_{Tg} = 0$. Then, we study R_{dev} as a function of V_{Tg} , shown in Fig. 3A (the balancing was done at $V_{Bg} = -28$ volts and $V_{Tg} = 0$). R_{dev} shows reproducible fluctuations throughout the whole range of V_{Tg} , which resemble mesoscopic con-

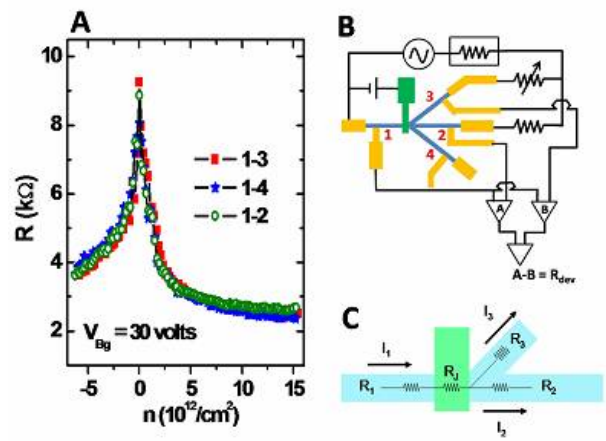


FIG. 2: (A) Resistance as a function of carrier density under the application of top gate voltage for arms 2, 3 and 4 on device SL1. The resistance on each arm was measured using standard four-probe technique with non-invasive leads. Nearly identical resistance curves as a function of V_{Tg} on all three arms reflects the fact that all three arms share the same gated portion. In order to reliably measure the difference between pairs of curves shown here, we use the balanced differential measurement technique shown in (B). (B) Measurement schematic used to isolate the angle-dependent portion of the resistance. In this schematic, the current branching in the arms 2 and 3 is balanced (using a variable resistor) in such a way that the voltage difference between A and B is zero when $V_{Tg} = 0$ (arm 4 is not connected on this schematic). The deviation from the balanced condition, ΔV is then measured as a function of V_{Tg} . In order to relate this measurement to the transmission probability, we define a parameter $R_{dev} = \Delta V(V_{Tg} = 0)/I_1$ with units of resistance. R_{dev} is then proportional to the difference in the transmission probability and reflects the current redistribution in the two leads as a function of V_{Tg} . (C) Current branching diagram for arms 2 and 3. R_1 and R_J denote resistances of arm 1 and the entire junction defined by the top gate, respectively. R_1 and R_J are both common to both current paths. The resistances of arms 2 and 3 can be further separated into ballistic and diffusive parts, so that $R_2 = R_{2b} + R_{2d}$ and $R_3 = R_{3b} + R_{3d}$. Here R_{2b} and R_{3b} denote the resistances of the portions of arms 2 and 3 that are within the mean free path of the junction, while R_{2d} and R_{3d} are the resistances of the rest of the arms 2 and 3.

ductance fluctuations [32] (the amplitude of the fluctuations in units of conductance are on the order of $0.01 e^2/h$). The amplitude of the fluctuations in R_{dev} visibly increases for positive values of V_{Tg} , when we expect a p-n-p junction to have formed. If we balance the circuit at $V_{Bg} = 25$ volts and $V_{Tg} = 0$, larger fluctuations in R_{dev} are observed below $V_{Tg} = -2$ volts, when we have an n-p-n junction formed under the top gate (see Fig. 3B). In order to emphasize the amplitude of these fluctuations, we examine the derivative of R_{dev} as a function of V_{Tg} (dR_{dev}/dV_{Tg}), as shown in Fig. 3C. dR_{dev}/dV_{Tg} is shown here as a function of V_{Tg} , along with the corresponding change in resistance of the entire path to illustrate the

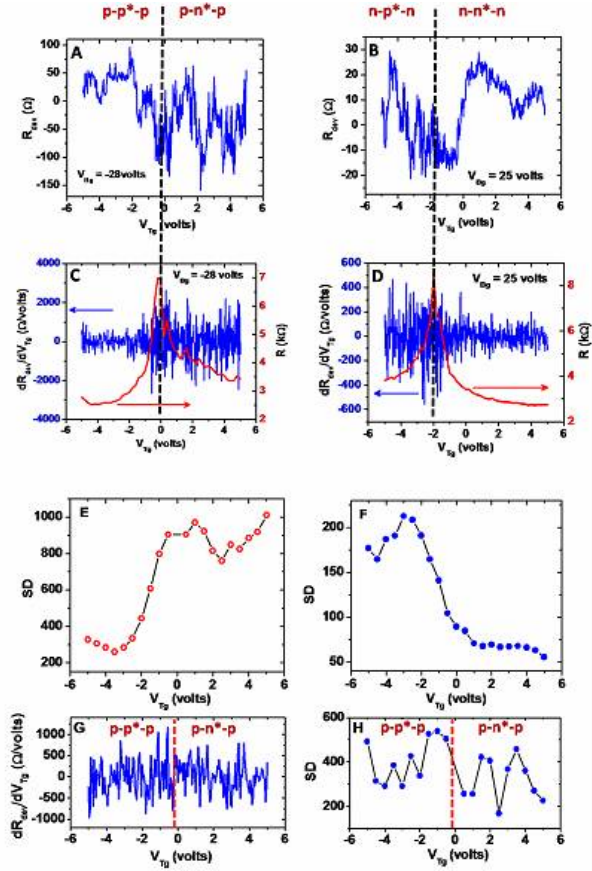


FIG. 3: R_{dev} as a function of V_{Tg} for (A) $V_{Bg} = -28$ volts and (B) $V_{Bg} = 25$ volts. R_{dev} is measured by balancing arms 2 and 3, as shown in the schematic in Fig. 2(B). Corresponding derivatives of R_{dev} with respect to V_{Tg} are shown in (C) for $V_{Bg} = -28$ volts and (D) for $V_{Bg} = 25$ volts (left axis). The corresponding change in resistance is shown in red (right axis). The amplitude of the fluctuations is visibly larger in the p-n-p and n-p-n regimes than in the p-p-p and n-n-n regimes. Standard deviation of $dR_{balance}/dV_{Tg}$ as a function of V_{Tg} is shown in (E) $V_{Bg} = -28$ volts and (F) $V_{Bg} = 25$ volts. The standard deviation of $dR_{balance}/dV_{Tg}$ increases up to four times as the variation of V_{Tg} takes the device from the p-p*-p to p-n*-p or from n-n*-n to n-p*-n regime. (G) A derivative of R_{dev} with respect to V_{Tg} and its standard deviation (H) measured by balancing arms 3 and 4 (both at $\pm 45^\circ$ with respect to arm 2) at $V_{Bg} = -28$ volts. No change is observed as the device enters the bipolar regime in this case.

proximity to the Dirac point. It is evident that the fluctuations are significantly larger in the p-n-p side than in the p-p-p side. Similarly, larger fluctuations are observed in the n-p-n side compared to the n-n-n side of the top gate voltage axis (Fig. 3D).

To obtain a more quantitative measure of the amplitude of these fluctuations, we divided the data points into small bins and calculated the standard deviation of dR_{dev}/V_{Tg} as a function of V_{Tg} . Figures 3E and 3F show the standard deviation calculated with twenty five data points per bin and averaged over four data points. It is

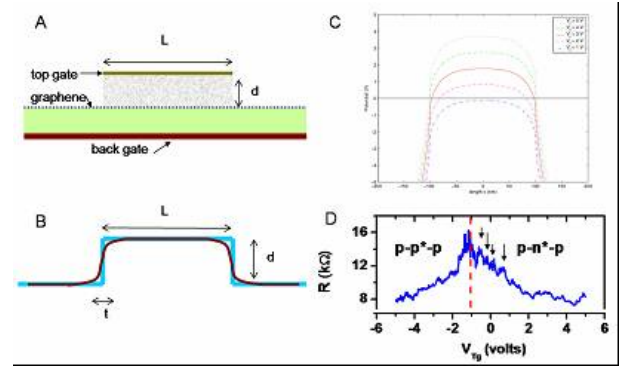


FIG. 4: (A) Side view schematic of the top gated portion of the sample. (B) Shape of the potential barrier formed by the top gate. (C) Potential profiles under the top gate calculated by solving the Laplace equation with appropriate boundary conditions. (D) Resistance as a function of V_{Tg} measured on the straight arm 2. The arrows point at the local peaks in the resistance.

evident that the standard deviation of the fluctuations increases by a factor of four as we cross from p-p-p to p-n-p or from n-n-n to n-p-n region (we note that the standard deviation of the fluctuations is overall larger when we have a p-n-p junction, than in the case of a n-p-n junction).

Similar results were obtained by comparing arms 2 and 4 (one straight and one angled). However, if we compare arms 3 and 4 (both at 45° angle with respect to the junction interface, we find that the variation in the R_{dev} remains nearly constant throughout the whole range of top and back gate voltages, as shown in Fig. 3G. This is also confirmed by the standard deviation shown in Fig. 3H.

There are two possible contributions to R_{dev} that could depend on V_{Tg} : mesoscopic conductance fluctuations and angle-dependent transmission. The balanced differential measurement cancels out any other contributions due to the size, geometry, and other contributions that do not depend on the gate voltage. Mesoscopic conductance fluctuations are indeed expected in samples of similar size [32]. These fluctuations are the consequence of quantum interference of electron wavefunctions scattered on impurities, and are reproducible as a function of gate voltage for a given impurity configuration. The top gate voltage in our sample does not affect the bulk of arms 2, 3 and 4, but it is likely to affect a small portion within the mean free path of the top gate. Since the top gate has a finite width, the impurity configuration along this width, while certainly similar, is not exactly identical. Therefore, dR_{dev} would measure the difference in conductance fluctuations in small ballistic portions of two different arms. This would manifest as random, but reproducible fluctuations in dR_{dev} as a function of V_{Tg} , as is indeed observed in our measurement in the entire range of V_{Tg} . In the case when a bipolar junction is formed under the

top gate, the fluctuations are visibly increased. To see whether this increase reflects enhanced mesoscopic conductance fluctuations, we examine the dR_{dev} measured by balancing different pairs of arms. Measuring all pairs of arms on three different devices, we find that increased fluctuations are observed only when the two arms are at a different angle - if we compare arms 3 and 4, the amplitude of the fluctuations remains the same throughout the whole range of V_{Tg} . We therefore conclude that the difference in the mesoscopic conductance fluctuations in the ballistic portions of the leads is the cause of the baseline fluctuations, but cannot account for the increase in the fluctuation amplitude (leading to the four-fold increase in the standard deviation) observed when a bipolar junction has formed under the top gate.

In order to examine the possibility that this increase is due to angle-dependent difference in the transmission detected on different arms of our devices, we need to consider the appropriate model for the potential barrier formed by the top gate (Fig 4A). A sharp, ballistic, rectangular barrier of length L and height d (shown in Fig. 4B in blue) would lead to perfect transmission at normal incidence and an oscillating transmission probability at other incident angles. A differential measurement of one straight and one angled arm would then result in oscillating resistance in the case of a bipolar junction, and no oscillations in the case of over-barrier transmission (p-p-p or n-n-n case). These oscillations would be superposed with the mesoscopic conductance fluctuations, resulting in increased fluctuation amplitude in the case of bipolar junction. This could, in principle, explain our results. However, given that the estimated mean free path is on the order of the top gate length, our devices are quasi-ballistic at best and it is not obvious that we can assume the potential to be sharp. Estimating the mean free path (l_{mfp}) from its relation to conductance $\sigma = 2(e^2/h)(k_F l_{mfp})$, we find it to be around ~ 100 - 200 nm in our samples ($l_{mfp} = 110$ nm for the sample shown in Fig 2 A, evaluated at 3V). The width of the top gate in all samples is 200 nm. Therefore, we cannot assume that the entire p-n-p structure is ballistic, but we can think of it as quasi-ballistic, as some portion of carriers is likely to pass through the barrier without scattering. Alternatively, we may have to treat the p-n-p junction as two p-n junctions in series, as discussed below. A realistic barrier, however, would not have infinitely sharp edges - we expect the potential to rise over some distance t (Fig. 4B). The edges can still be considered sharp if the electron wavelength is large compared to t , or if $k_F t < 1$. In our samples, $k_F t \sim 10$ (taking $k_F = \sqrt{\pi n}$ at 3V, away from the Dirac point), so we need to consider smooth edges.

Another important consideration is whether transport through each p-n junction is ballistic or diffusive. A good measure for this is a parameter $\beta = n'/n_i^{2/3}$, where n' is the density gradient at zero energy, and n_i is a parame-

ter related to mobility through $n_i = e/h\mu$ [25]. In order to observe ballistic transport through a p-n junction, it is required that $\beta > 10$. The mobility can be estimated from $\mu = 1/en\rho(n)$, where n is the carrier density and $\rho(n)$ is the resistivity of the sample away from the Dirac point. The mobility in our samples is ~ 2800 cm²/Vs, and the top gate is placed at the height $d=20$ nm away from graphene, as shown in Fig. 4B. The distance over which the potential increases at the p-n interface, t , can be taken to be on the order of d . Estimating the density gradient at the interface from the difference in the carrier densities on the two sides of each p-n junction over 20nm, we arrive at the value of $\beta \sim 160$, indicating that we should expect a significant ballistic contribution. This is confirmed by the calculation of the potential profiles under the top gate, shown in Fig. 4C.

A model for smooth ballistic p-n junctions was developed in reference [8]. This model predicts that a smooth p-n junction transmits only the carriers that approach it within a small incident angle θ smaller than $\theta_0 = (\pi k_F t)$. The transmission probability as a function of the incident angle is [8]: $T(\theta) = e^{-\pi(k_F t \sin^2 \theta)}$ so we would expect perfect transmission for normally incident carriers, and suppressed transmission with increasing incident angle. In our samples $\theta_0 = 6^\circ$, so we would expect efficient collimation within the mean free path away from the p-n interface. Our p-n-p (or n-p-n) junctions include two p-n interfaces - one on either edge of the top gate. The first p-n junction would then preferentially transmit more carriers that are nearly normally incident to the barrier. These carriers would arrive to the second p-n junction, which would again select more of the normally incident ones. As all the arms have the same width, and the branching point is less than l_{mfp} away from the top-gated portion, most of the electrons coming from arm 1, that emerged in the direction normal to the second pn junction, will go straight into arm 2. The arm 3 (or 4) is placed at an angle with respect to the top gate ($\phi = 45^\circ$), so it will preferentially collect any electrons that emerged at angles close to $\phi = 45^\circ$. Here we also have to take into account the fact that the arms have a finite width, and the electrons can emerge anywhere along that width. Therefore, each arm will actually collect electrons that emerge at a small range of angles.

If we assume that the carriers tunnel through two independent p-n junctions in series, than we would expect most of the carriers to be collected by arm 2, with very few carriers going into arm 3 or 4. In this case, we would not expect to see oscillations in the transmission amplitude as a function of barrier height.

If, however, the transport through the p-n-p junction is coherent, one can expect to observe resonant tunneling through quasi-bound states due to Fabry-Perot interference [11, 20]. In this case, the oscillating part of the

resistance can be approximated by [11, 20]:

$$R_{osc}^{-1} = \frac{8e^2}{h} \sum [T^4(1 - T^2) \cos \theta_{WKB} e^{-\frac{2L}{l_{mfp}}}] \quad (1)$$

where T is the transmission coefficient and θ_{WKB} is the semiclassical phase [11, 20]. Taking into account non-linear screening when evaluating T [26], this expression results in resistance oscillations with an approximate period in the carrier density of about 10^{12} cm^{-2} . In our samples, this would result in oscillations with V_{Tg} with a period of about 0.5V, which is indeed observed in four-terminal measurements of resistance on arm 2, as shown in Fig 4D. These oscillations are superimposed with the mesoscopic conductance fluctuations, as expected from Fabry-Perot resonances in the presence of disorder [16]. In the presence of disorder, it was found that the oscillations survive even at impurity concentrations that are by an order of magnitude larger than that observed in our samples, but become smeared by mesoscopic conductance fluctuations. Such fluctuations, in addition to inhomogeneous gate coupling due to the disorder, were also found to cause averaging over several Fabry-Perot fringes in all but the cleanest samples [20]. In this picture, small-angle averaged irregular oscillations would be expected on arm 2 when a bipolar junction is formed under the top gate, with very few carriers making it to arm 3 or 4. Comparing arm 2 with either 3 or 4 would then result in the increased oscillation amplitude, while comparing arms 3 and 4 would not, as observed in our experiment.

We note that it is not necessary for the entire device to be ballistic in order to observe the angle dependence of the resistance. As long as the difference in the current distribution due to ballistic effects in a small portion of the straight and angled arms is large enough, it will manifest as the deviation from the balanced condition with changing top gate voltage. Therefore, our measurement technique specifically *selects* and only measures the ballistic contribution. Since all the arms share the same top-gated portion, the properties of the potential barrier are identical for straight and angled arms: there will be no differences in the pn-junction length, roughness, the nature of disorder, contact resistance and other issues that have to be taken into account when comparing different physical devices.

In conclusion, even though our measurements were limited by mesoscopic conductance fluctuations, we were able to observe angle-dependent transmission through a p-n-p junction in graphene. Using cleaner samples with higher mobility and a larger mean free path would make it possible to make more detailed angle-resolved measurements, which could lead to electron optics applications.

[1] Novoselov K. S., Geim A. K., Morozov S. V., Jiang D., Zhang Y., Dubonos S. V., Grigorieva I. V., & Firsov A.

- A. Electric field effect in atomically thin carbon films. *Science* **306**, 666-669 (2004).
- [2] Geim A. K., & Novoselov K. S., The rise of graphene. *Nat. Mater.* **6**, 183-191 (2007).
- [3] Castro Neto A. H., Guinea F., Peres N. M. R., Novoselov K. S. & Geim A. K. The electronic properties of graphene. *Rev. Mod. Phys.* **81**, 109-162 (2009).
- [4] Das Sarma S., Adam S., Hwang E. H. & Rossi E. Electronic transport in two-dimensional graphene. *Rev. Mod. Phys.* **83**, 407-470 (2011).
- [5] Ando T., Nakanishi T., & Saito R. Berry's Phase and Absence of Back Scattering in Carbon Nanotubes. *J Phys. Soc. Jpn.* **67**, 2857-2862 (1998).
- [6] Suzuura H., & Ando T. Crossover from Symplectic to Orthogonal Class in a Two-Dimensional Honeycomb Lattice. *Phys. Rev. Lett.* **89**, 266603 (2002).
- [7] Beenakker C. Andreev reflection and Klein tunneling in graphene. *Rev. Mod. Phys.* **80** 1337-1354 (2008).
- [8] Cheianov V. V., & Fal'ko V. I. Selective transmission of Dirac electrons and ballistic magnetoresistance of n-p junctions in graphene *Phys. Rev. B* **74** 041403 (2006).
- [9] Cheianov V. V., Fal'ko V. I., & Altshuler B. L. The Focusing of Electron Flow and a Veselago Lens in Graphene p-n Junctions. *Science* **315**, 1252-1255 (2007).
- [10] Katsnelson M. I., Novoselov K. S., & Geim A. K. Chiral tunnelling and the Klein paradox in graphene. *Nat. Phys.* **2**, 620-625 (2006).
- [11] Shytov A. V., Rudner M. S., & Levitov L. S. Klein Backscattering and Fabry-Perot Interference in Graphene Heterojunctions. *Phys. Rev. Lett.* **101**, 156804 (2008).
- [12] Park C.-H., Son Y.-W., Yang L., Cohen M. L., & Louie S. G. Electron Beam Supercollimation in Graphene Superlattices. *Nano. Lett.* **8**, 2920-2924 (2008).
- [13] Beenakker, C. W. J., Sepkhanov, R. A., Akhmerov, A. R. & Tworzydło, J. Quantum Goos-Hänchen effect in graphene. *Phys. Rev. Lett.* **102**, 146804 (2009).
- [14] Hartmann, R. R., Robinson, N. J. & Portnoi, M. E. Smooth electron waveguides in graphene. *Phys. Rev. B* **81**, 245431 (2010).
- [15] Low T. & Appenzeller J. Electronic transport properties of a tilted graphene p-n junction. *Phys. Rev. B* **80**, 155406 (2009).
- [16] Rossi E., Bardarson J. H. Brouwer P. W. & Das Sarma S. Signatures of Klein tunneling in disordered graphene p-n-p junctions *Phys. Rev. B* 2010, **81**, 121408 (2010).
- [17] Sajjad R. & Ghosh A. High efficiency switching using graphene based electron optics *Appl. Phys. Lett.* **99**, 123101 (2011).
- [18] Huard B., Sulpizio J. A., Stander N., Todd K., Yang B., & Goldhaber-Gordon D. Transport Measurements Across a Tunable Potential Barrier in Graphene. *Phys. Rev. Lett.* **98**, 236803 (2007).
- [19] Stander N., Huard B., & Goldhaber-Gordon D. Evidence for Klein Tunneling in Graphene p-n Junctions. *Phys. Rev. Lett.* **102**, 026807 (2009).
- [20] Young A. F., & Kim P. Quantum interference and Klein tunnelling in graphene heterojunctions. *Nat. Phys.* **5**, 222-226 (2009).
- [21] Wu Y., Perebeinos V., Lin Y.-M., Low T., Xia F., & Avouris P. Quantum Behavior of Graphene Transistors near the Scaling Limit. *Nano. Lett.* **12**, 1417-1423 (2012).
- [22] Gorbachev R. V., Mayorov A. S., Savchenko A. K., Horsell D. W., & Guinea F. Conductance of p-n-

- p Graphene Structures with "Air-Bridge" Top Gates. *Nano. Lett.* **8**, 1995-1999 (2008).
- [23] Williams J. R., Low T., Lundstrom M. S., & Marcus C. M. Gate-controlled guiding of electrons in graphene. *Nat. Nano.* **6**, 222-225 (2011).
- [24] Sutar S., Comfort E. S., Liu J., Taniguchi T., Watanabe K., & Lee J. U. Angle-Dependent Carrier Transmission in Graphene pn Junctions. *Nano. Lett.* **12**, 4460-4464 (2012).
- [25] Fogler M. M., Novikov D. S., Glazman L. I., & Shklovskii B. I. Effect of disorder on a graphene p-n junction. *Phys. Rev. B* **77**, 075420 (2008).
- [26] Zhang L. M., & Fogler M. M. Nonlinear Screening and Ballistic Transport in a Graphene p-n Junction. *Phys. Rev. Lett.* **100**, 116804 (2008).
- [27] Sonin E. B. Effect of Klein tunneling on conductance and shot noise in ballistic graphene. *Phys. Rev. B* **79**, 195438 (2009).
- [28] Xia F., Perebeinos V., Lin Y.-M., Wu Y., & Avouris P. The origins and limits of metal-graphene junction resistance. *Nat. Nano.* **6**, 179-184 (2011).
- [29] Giovannetti G., Khomyakov P. A., Brocks G., Karpan V. M., van den Brink J., & Kelly P. J. Doping Graphene with Metal Contacts. *Phys. Rev. Lett.* **101**, 026803 (2008).
- [30] Lee E. J. H., Balasubramanian K., Weitz R. T., Burghard M., & Klaus Kern K. Contact and edge effects in graphene devices. *Nat. Nano.* **3**, 486-490 (2008).
- [31] Huard B., Stander N., Sulpizio J. A., & Goldhaber-Gordon D. Evidence of the role of contacts on the observed electron-hole asymmetry in graphene. *Phys. Rev. B* **78**, 121402(R) (2008).
- [32] Tikhonenko F. V., Horsell D. W., Gorbachev R. V., & Savchenko A. K., Weak localization in graphene flakes. *Phys. Rev. Lett.* **100**, 056802 (2008).